Selective and Reversible Noncovalent Functionalization of Single-Walled Carbon Nanotubes by a pH-Responsive Vinylogous Tetrathiafulvalene–Fluorene Copolymer

Shuai Liang,[†] Yuming Zhao,[‡] and Alex Adronov*,[†]

[†]Department of Chemistry, McMaster University, Hamilton, Ontario, Canada L8S 4M1
[‡]Department of Chemistry, Memorial University of Newfoundland, St. John's, Newfoundland, Canada A1B 3X7

S *Supporting Information*

ABSTRACT: A vinylogous tetrathiafulvalene (TTFV) monomer was prepared and copolymerized with fluorene to give a conformationally switchable conjugated copolymer. This copolymer was shown to undergo a conformational change upon protonation with trifluoroacetic acid (TFA). When mixed with single-walled carbon nanotubes (SWNTs), this TTFV–fluorene copolymer exhibited strong interactions with the SWNT surface, leading to stable, concentrated nanotube dispersions in toluene. Photoluminescence excitation mapping indicated that the copolymer selectively disperses low-diameter

SWNTs, as would be expected from its ability to form a tightly coiled conformation on the nanotube surface. Addition of TFA to the copolymer–SWNT dispersion resulted in a rapid conformational change and desorption of the polymer from the SWNT surface, resulting in precipitation of pure SWNTs that were completely free of polymer. Importantly, the nanotubes isolated after dispersion and release by the TTFV–fluorene copolymer were more pure than the original SWNTs that were initially dispersed.
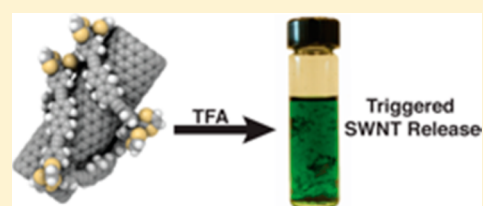
■ INTRODUCTION

Functionalization of single-walled carbon nanotubes (SWNTs) enables their homogeneous dispersion in various solvents and bulk materials.[1−10] Of the recently reported functionalization strategies, supramolecular approaches have the advantage of producing concentrated dispersions without deteriorating the conjugated sidewall structure of SWNTs.[11−13] This enables retention of their unique structural, electronic, thermal, optical, and mechanical properties and improves their applicability within devices.[14−17] Conjugated polymers have been extensively used as supramolecular adducts and dispersion agents, as they form multiple π-stacking interactions with the nanotube surface, leading to strong interactions.[18−24] In this respect, it has also been shown that rationally designed conjugated polymers, such as poly(9,9-dialkylfluorene)s, are capable of selectively interacting with specific, mostly semiconducting, nanotube species.[25−30] These observations have spawned a significant effort in determining design rules for conjugated polymers such that their selectivity toward specific nanotube types is optimized, with the vision of isolating pure fractions of specific SWNTs.[15,31−33]

Although selective interactions between conjugated polymers and SWNTs have allowed isolation of specific SWNT chiralities, the purified SWNTs still retain the conjugated polymer on their surface.[23,26,34] It has been shown that removal of the surface-bound polymer via solvent washing is difficult, as the interaction with the SWNT surface is very strong and prevents polymer desorption.[24] Recent studies have also demonstrated that application of polymer–SWNT complexes within field effect transistor (FET) devices results in decreased

on-current and on/off ratio, relative to those of devices prepared with pristine SWNTs that are not coated with polymers.[35] Thus, strategies for achieving strong and selective interactions between conjugated polymers and SWNTs to produce concentrated dispersions of specific nanotube chiralities, combined with reversible complexation such that the polymer can be desorbed from the nanotube surface upon application of a specific stimulus, are required.[36]

Recently, a class of novel vinylogous tetrathiafulvalene–phenylacetylene copolymers was shown to disperse SWNTs in organic solvents.[37,38] These copolymers exhibited reversible conformational switching behavior upon oxidation/reduction of the tetrathiafulvalene vinylogue (TTFV) units, which resulted in a redox-mediated release of SWNTs. However, the low molecular weights and poor solubility of the copolymers resulted in low SWNT concentrations dispersed in solution, and the overall copolymers did not show appreciable selectivity for specific SWNT chiralities. To address these issues, we hypothesized that introduction of highly π-conjugated aromatic units in the TTFV polymer backbone would assist in addressing these shortcomings. In previous studies, fluorene-based polymers have been found to show excellent efficiency and selectivity in SWNT dispersion.[26] Here, we report the preparation of a TTFV–fluorene copolymer that exhibits strong interactions with SWNTs and imparts selectivity as a result of incorporation of the fluorene monomer unit. This novel copolymer is also capable of reversible SWNT binding

Scheme 1. Synthesis of TTFV−Fluorene Copolymer 7
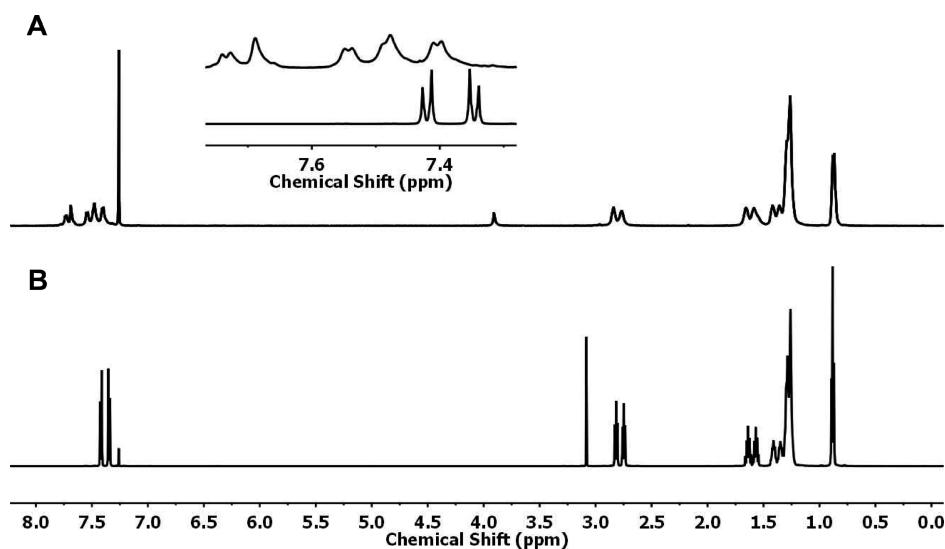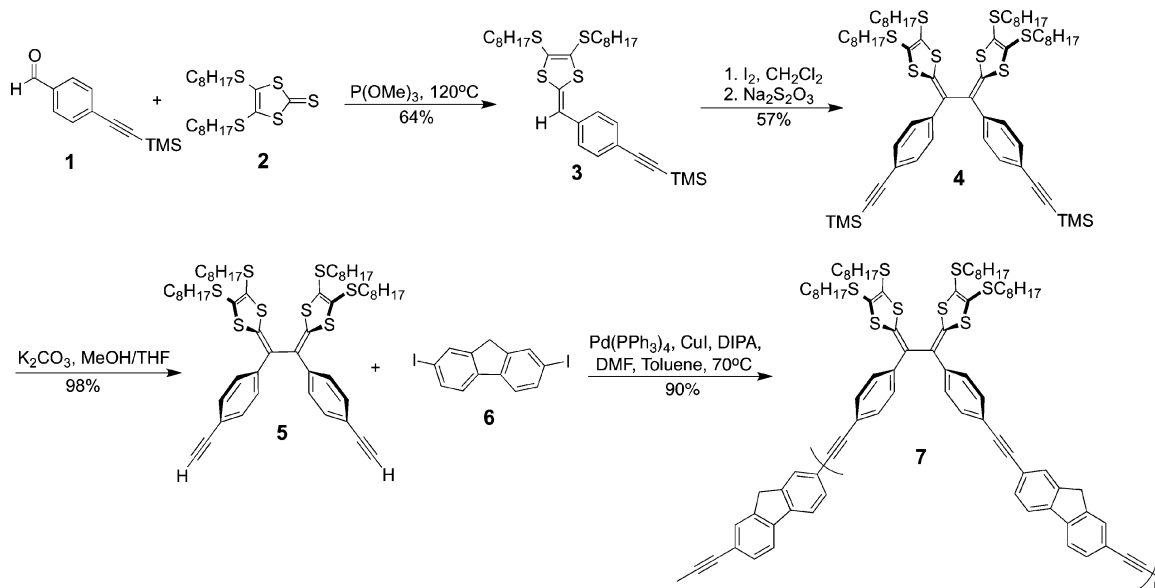
Figure 1. ^{1}H NMR (600 MHz, CDCl$_3$) spectra for (A) the copolymer **7** and (B) TTFV precursor **5**. The inset shows a comparison of the magnified aromatic regions for the copolymer **7** (top) and the TTFV monomer **5** (bottom).

and was shown to release SWNTs upon protonation of the TTFV unit with trifluoroacetic acid (TFA).

■ RESULTS AND DISCUSSION

Synthesis of the TTFV−fluorene copolymer was carried out according to Scheme 1. Compounds **1** and **2** were prepared following literature procedures.[39] Phosphite-mediated coupling of **1** and **2** afforded the phenyl dithiafulvene **3**, which was subsequently subjected to an iodine-promoted oxidative dimerization followed by reductive workup with Na$_2$S$_2$O$_3$ to produce the neutral phenylacetylene-substituted TTFV compound **4**. Removal of the trimethylsilyl (TMS) groups of **4** under basic conditions gave the free terminal bisalkyne product **5**, which was subsequently subjected to a Sonogashira cross-coupling polymerization with 1 equiv of 2,7-diiodofluorene (**6**), catalyzed by Pd(PPh$_3$)$_4$ and CuI with diisopropylamine (DIPA) as base. The resulting TTFV−fluorene copolymer **7** was isolated as a yellow solid, which was reasonably soluble in
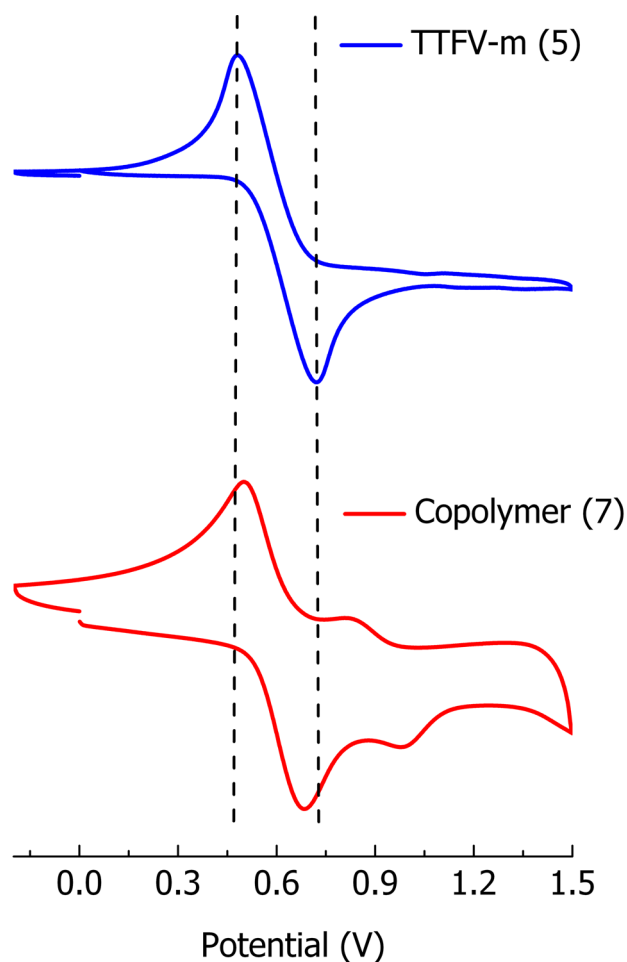
nonpolar organic solvents such as toluene, THF, and chloroform. Gel permeation chromatographic (GPC) analysis of copolymer **7** revealed a number-average molar mass (M_n) of 19 000 g/mol and a polydispersity index (PDI) of 1.8, relative to polystyrene standards. Characterization of copolymer **7** by ^{1}H NMR spectroscopy confirmed the 1:1 ratio of the TTFV and fluorene units within the structure. As expected, the protons of the phenyl rings of TTFV shift from 7.42 and 7.35 ppm in the monomer (Figure 1B) to 7.48 and 7.41 ppm in the copolymer (Figure 1A).

The electronic absorption properties of copolymer **7**, the fluorene precursor **6**, and the TTFV precursor **5** were investigated by UV−vis absorption spectroscopy (Figure 2). From these data, it can be seen that the copolymer's absorption maximum ($\lambda_{max} = 407$ nm) is red-shifted significantly from that of either monomer ($\lambda_{max} = 314$ and 377 nm for fluorene and TTFV-m monomer **5**, respectively), indicating that delocalization of electrons has occurred within the copolymer as a result
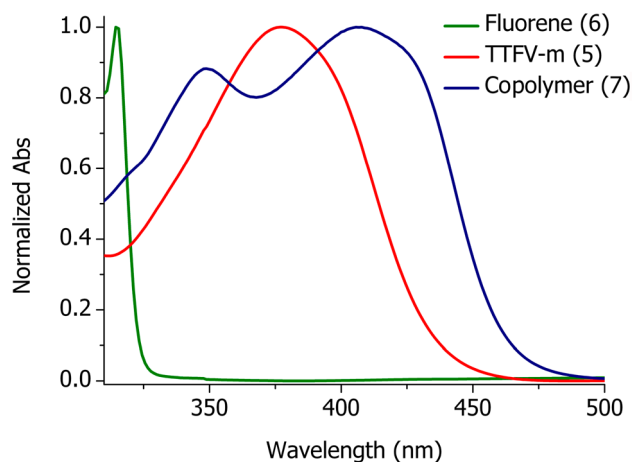
Figure 2. UV−vis absorption spectra for the fluorine precursor **6**, the TTFV-m monomer **5**, and the copolymer **7**. Spectra were measured in CH_2Cl_2 at room temperature.

of π-conjugation between the constituent units. The electrochemical properties of the TTFV-m monomer **5** and copolymer **7** were investigated by cyclic voltammetry (CV) in CH_2Cl_2 at room temperature. The measured cyclic voltammograms are shown in Figure 3. The CV profile for TTFV-m **5** shows a reversible redox wave pair at +0.48 and +0.72 V, attributed to a

characteristic simultaneous two-electron transfer process occurring on the diphenyl-TTFV unit that assumes a pseudo-*cis* conformation in the neutral state.[39] The actual molecular geometry of TTFV in the neutral state has been unambiguously elucidated by X-ray single-crystal structural analysis,[40−43] which reveals a twisted pseudo-*cis* molecular structure. The CV data for copolymer **7** exhibit similar features for the reduction and oxidation of the TTFV-m unit, though the peaks are broadened and peak maxima are shifted closer together, located at +0.50 and +0.68 V, as a result of the increased conjugation within the copolymer. An additional redox couple at +0.81 and +0.98 V is also observed for the copolymer, which possibly arises from a minor *trans* conformer of the TTFV-m unit within the copolymer structure.[44] These CV data are consistent with the copolymer structure of **7**.

Treatment of copolymer **7** with trifluoroacetic acid TFA resulted in the formation of TTFV mono- and dications, which exhibit distinct electronic absorption features. Like other known TTFV derivatives, the protonation of copolymer **7** occurs via a two-step process, where the formation of TTFV monocation and dication takes place sequentially.[38] This is evidenced by UV−vis titration analysis (Figure 4) where a solution of copolymer **7** was titrated with TFA up to 2250 equiv. The UV−vis titration data clearly show spectroscopic changes occurring

Figure 3. Cyclic voltammograms of TTFV-m monomer **5** and copolymer **7**.
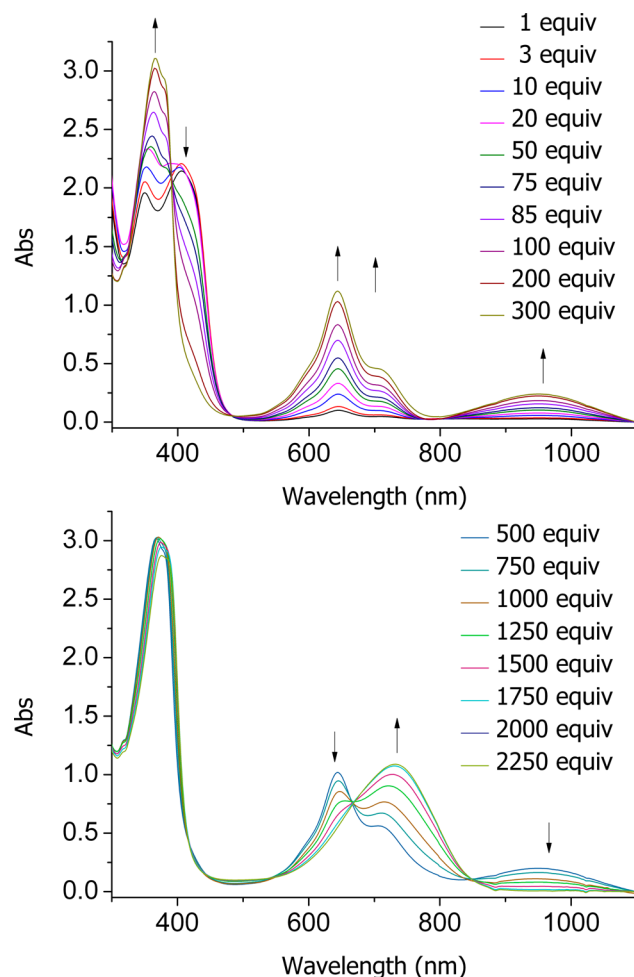
Figure 4. UV−vis spectral changes monitoring the titration of copolymer **7** with TFA (top, from 1 to 300 equiv of TFA; bottom, from 500 to 2250 equiv of TFA). All titration experiments were done in CH_2Cl_2 at room temperature.

in two stages. In the first stage (up to 300 equiv of TFA), the intensity of the absorption band at 405 nm, which is attributed to the $\pi-\pi^*$ transition of neutral TTFV, continuously decreases with increasing acidity. Simultaneously, two new longer wavelength absorption bands at 643 and 948 nm emerge and grow steadily. These two bands are consistent with the known UV−vis absorption features of TTF radical cations,[45] and hence are assigned to the monoprotonated $[TTFV \cdot H]^+$. In addition, a shoulder at 710 nm is observable in this process, which is attributed to partial formation of the dication $[TTFV \cdot 2H]^{2+}$. As the acidification continues, the formation of the dication leads to further spectral changes, where the two bands at 643 and 948 nm (attributed to $[TTFV \cdot H]^+$) diminish and the band at 710 nm (attributed to $[TTFV \cdot 2H]^{2+}$) grows significantly (Figure 4). Since the final diprotonated $[TTFV \cdot 2H]^{2+}$ units have been known to undergo a conformational switch to the *trans* conformation to minimize charge repulsions,[46] the entire conformation of protonated polymer 7 is predicted to take a linear structure. This acidity-responsive conformational change serves as the driving force for effective release of SWNTs from the corresponding polymer−SWNT assemblies (see below).

Molecular Modeling Studies. Molecular structural properties of copolymer 7 as well as the complex of 7 with a (10,0) SWNT were investigated by molecular mechanics calculations using the SYBYL force field implemented with the Spartan'10 software package (the alkyl chains on TTFV were replaced with H atoms for clarity and computational simplification). The calculated conformations indicate that the free polymer has a relatively flexible backbone and tends to form an irregular folded conformation, in which the TTFV units take a pseudo-*cis* geometry similar to those of diphenyl-TTFV derivatives determined by X-ray crystallography (Figure 5A,B).[46] However, upon interacting with SWNTs, the polymer
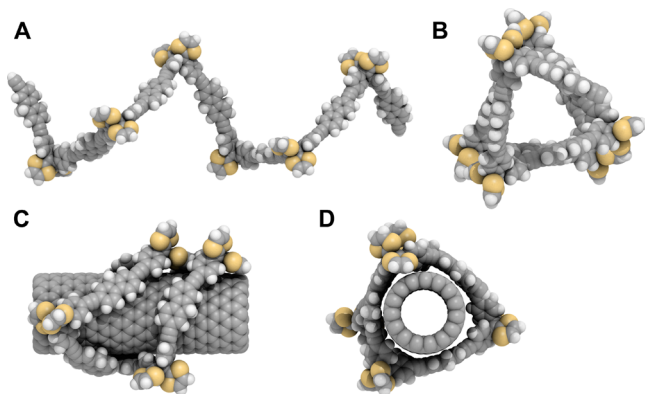

Figure 5. Conformation of a model hexamer of TTFV−fluorene copolymer: (A) side view, (B) front view. Two projections of the conformation of a model hexamer wrapping around a (10,0) SWNT: (C) side view, (D) front view.

adopts a more tightly packed helical conformation that exhibits a 1.5 nm diameter hollow inner cavity that is well suited for wrapping an exfoliated (10,0) SWNT (ca. 1.1 nm in diameter) via $\pi-\pi$ interactions (Figure 5C,D). It is worth noting that all the fluorene units show direct face-to-face contact with the surface of the SWNT, suggesting that the fluorene−SWNT π-stacking contributes the most significant driving force for the polymer to wrap around an individual SWNT.

Dispersion of SWNTs with the TTFV−Fluorene Copolymer. The ability of copolymer 7 to form supramolecular complexes with SWNTs and enable their homogeneous dispersion in organic solvents was investigated using previously published protocols.[37] Briefly, 3 mg of raw SWNT powder (CoMoCat or HiPco) was added to a polymer solution containing 50 mg of polymer dissolved in 10 mL of toluene. The polymer−SWNT mixtures were sonicated for 30 min in a bath sonicator that was chilled with ice, followed by 60 min of centrifugation at 8346g. The supernatant was carefully removed from the centrifuge tube to obtain a stable dispersion of the 7−SWNT complexes. This dispersion was extremely dark and stable with no observable flocculation over several months. The formation of these stable, concentrated dispersions is consistent with the theoretical predictions that the copolymer can adopt a suitable helical conformation to tightly wrap individual SWNTs (see above). Analysis by UV−vis−NIR spectroscopy revealed the presence of SWNT absorption bands in the wavelength range of 500−1500 nm, consistent with the presence of a high concentration of exfoliated SWNTs (Figure 6).[47] In the
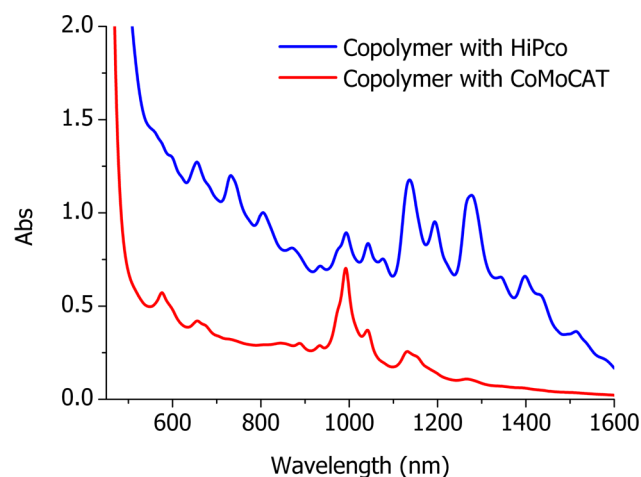

Figure 6. UV−vis−NIR absorption spectra for copolymer 7−HiPco dispersion (blue trace) and copolymer 7−CoMoCAT dispersion (red trace) in toluene.

absorption spectrum of the CoMoCAT SWNT dispersion, a prominent absorption peak at 999 nm was observed, which is assigned to SWNTs with a chiral index of (6,5).[48] Lower intensity absorptions corresponding to the (7,5) and (8,3) SWNTs were also observed.[48] In addition, the lack of background absorbance across the entire spectrum indicates that these samples do not contain significant amounts of amorphous carbon and SWNT aggregates. This suggests that complexation with copolymer 7 enables purification and debundling of commercial SWNT samples. The analogous absorption spectrum of the HiPco SWNT dispersion exhibits well-resolved peaks in the S_{11} (approximately 830−1600 nm) and S_{22} (approximately 600−830 nm) ranges, with very little signal corresponding to M_{11} transitions (450−650 nm) observable. However, overlap with the copolymer absorption in the M_{11} region makes it difficult to conclusively determine the extent to which metallic SWNTs are present in this dispersion.

Photoluminescence excitation (PLE) mapping is a powerful tool for characterizing different chiralities in bulk SWNT samples. The PLE maps for both CoMoCAT and HiPco

SWNTs dispersed by copolymer **7** in toluene are shown in Figure 7. On the basis of the high emission intensity observed
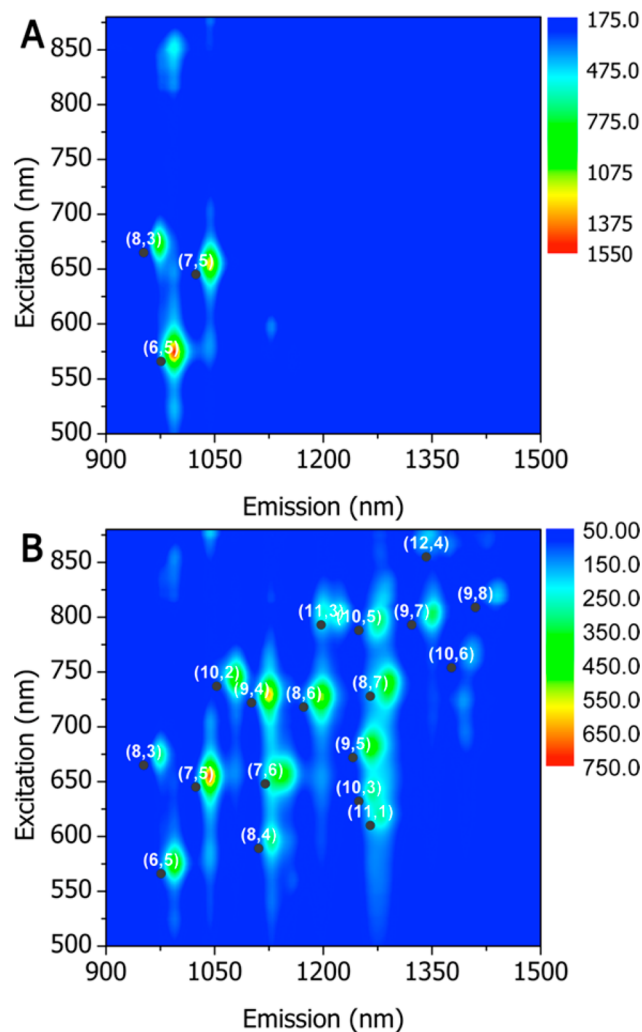
Figure 7. PLE maps of CoMoCAT (A) and HiPco (B) SWNTs dispersed in toluene with copolymer **7**.

for the SWNTs, it can be concluded that the copolymer efficiently debundled both CoMoCAT and HiPco bundles into individual, polymer-wrapped tubes. Although the intensity of signals in the PLE maps does not provide a quantitative measure of the SWNT concentration because the quantum efficiency of a given nanotube chirality may depend on its environment, it is still a useful indicator of a given polymer's selectivity for specific SWNTs when considered together with absorption data. On the basis of the PLE data in Figure 7, the **7**–CoMoCAT dispersion predominantly contains the (6,5) nanotube species, which is consistent with the UV−vis−NIR absorption data, while the **7**–HiPco dispersion predominantly contains the (7,5) SWNT species, although a number of other nanotube chiralities, including (9,4), (8,6), (6,5), (8,7), (9,5), (7,6), and (10,2), are also present (Figure 8). These major components in the **7**–HiPco dispersion are all low-diameter SWNTs (1.03 nm or lower), indicating that a certain degree of diameter selectivity is achieved with copolymer **7**. Considering the tight helical conformation that it is expected to adopt, it is not surprising that selective interactions based on nanotube diameter would be possible. The chiral angles of the eight
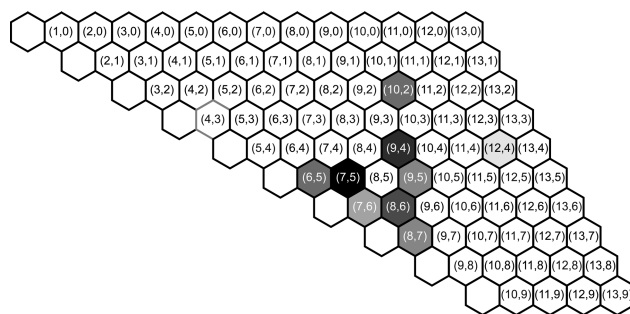
Figure 8. Graphene sheet maps showing normalized PL intensities for copolymer **7**–HiPco complexes. The darker fill shading represents higher PL intensity.

highest intensity signals from the **7**–HiPco dispersion are also listed in Table 1, and although most of these SWNTs have

**Table 1. Table of Chiral Index vs Diameter and Chiral Angle**

chiral index (*m,n*)	diameter (nm)	chiral angle (θ)	chiral index (*m,n*)	diameter (nm)	chiral angle (θ)
(8,7)	1.032	27.80	(7,6)	0.895	27.46
(9,5)	0.976	20.63	(10,2)	0.884	8.95
(8,6)	0.966	25.28	(7,5)	0.829	24.50
(9,4)	0.916	17.48	(6,5)	0.757	27.00

chiral angles above 24°, the presence of several species with lower chiral angles indicates that there is little chiral angle selectivity with this polymer. It is also interesting to compare the PLE map of **7**–HiPco to what is obtained when the same HiPco SWNTs are dispersed with a nonselective surfactant, such as sodium dodecylbenzenesulfonate (SDBS) (see the Supporting Information, Figure S1). Most notably, the (7,5) species that is prominent in the dispersion with the copolymer is a relatively minor component in the SDBS dispersion, indicating that copolymer **7** is indeed selective for specific SWNT types.

Tapping mode atomic force microscopy (AFM) was carried out on copolymer−SWNT complexes that were spin-cast onto freshly cleaved mica substrates. To observe individual SWNTs and eliminate the presence of free polymer, copolymer−SWNT samples were filtered through a Teflon membrane (0.2 μm pore diameter) and washed extensively until the filtrate contained no detectable free polymer. The resulting residue was dispersed in toluene, as described above, and used for sample preparation. Figure S2 (Supporting Information) shows the AFM image for the **7**–CoMoCAT complex, spin-cast from a 100-fold-diluted dispersion in toluene. From the image, it is clear that individual polymer-wrapped nanotubes are present. Height analysis of the AFM images indicates that the majority of nanotube features are approximately 2.5−3.2 nm high, which is consistent with single nanotube structures wrapped with a monolayer of polymer. Unfortunately, even after the extensive washing procedure, some features that resemble free polymer on the mica surface are still observable by AFM.

Release of SWNTs from Copolymer. As shown in Figure 4, the addition of acid to a solution of copolymer **7** leads to a significant change in its absorption properties and a dramatic conformational switch resulting from *cis*−*trans* isomerization of the TTFV units. Similarly, addition of two drops of TFA to a dispersion of the **7**–CoMoCAT SWNT complex at room temperature, followed by agitation of the vial to mix the

contents, resulted in an immediate color change of the polymer−SWNT dispersion from dark brown to green, accompanied by a simultaneous precipitation of the dispersed SWNTs (Figure 9 and Figure S3 of the Supporting
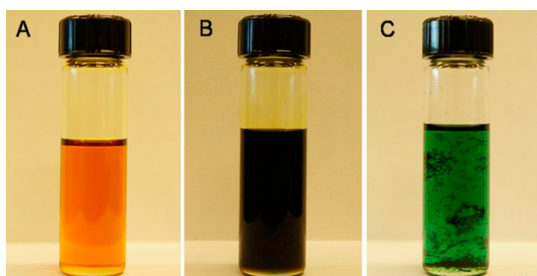
Figure 9. Photograph of (A) pure copolymer **7** solution in toluene, (B) a dispersion of copolymer **7**−CoMoCAT SWNTs in toluene, and (C) the dispersion after addition of TFA, showing precipitated nanotubes (the sample was diluted 4-fold to clearly see the precipitates).

Information). Clearly, the conformational change of the TTFV units leads to a polymer conformation that is not conducive to interaction with the SWNT surface. The released SWNTs were easily removed from the polymer solution via either filtration or centrifugation. The isolated acidified polymer solution was then treated with aqueous $NaHCO_3$ to neutralize the polymer and recover the original, orange solution of copolymer **7**. ^{1}H NMR analysis of the recovered polymer confirmed that there were no changes in its molecular structure as a result of nanotube complexation, release, and neutralization steps (Figure S4, Supporting Information). This recovered polymer could again be used to redisperse the precipitated SWNTs, demonstrating that the dissolution−precipitation process is reversible (Figure S5, Supporting Information).

Characterization of the released and isolated SWNTs was initially conducted using Raman spectroscopy. In particular, the radial breathing mode (RBM) signals[49] of SWNTs are strongly dependent on the nanotube diameter as well as any surface-adsorbed chemical species.[50−52] Raman data using 785 nm excitation were acquired for the CoMoCat SWNT starting material, the **7**−CoMoCat complexes, and the CoMoCat SWNTs recovered after release from the copolymer (Figure 10). The corresponding Raman data for the **7**−HiPco complexes are provided in the Supporting Information (Figure S6). For comparison, we also attempted to measure the Raman spectrum of the pure polymer at the same excitation wavelength, but only observed background signals from the silicon substrate (Figure S7, Supporting Information). In the RBM region, the CoMoCat starting material exhibits three prominent signals at 230, 264, and 301 cm^{-1} (Figure 10B). The signal at 264 cm^{-1} is often referred to as a "bundling peak", as it arises when nanotubes are aggregated in bundles.[53−55] Upon complexation with copolymer **7**, the bundling peak at 264 cm^{-1} dramatically decreases in intensity as a result of the exfoliation that occurs when the copolymer interacts with the SWNTs. More interestingly, the signal at 230 cm^{-1} undergoes a red shift by 3 cm^{-1}, indicating that a π-stacking interaction has occurred between the adsorbed polymer and the nanotube surface. Furthermore, the shoulder at 225 cm^{-1} increased in intensity relative to the peak at 230 cm^{-1}, possibly signifying enrichment in this SWNT species. The spectrum corresponding to the released SWNTs after polymer isomerization shows the
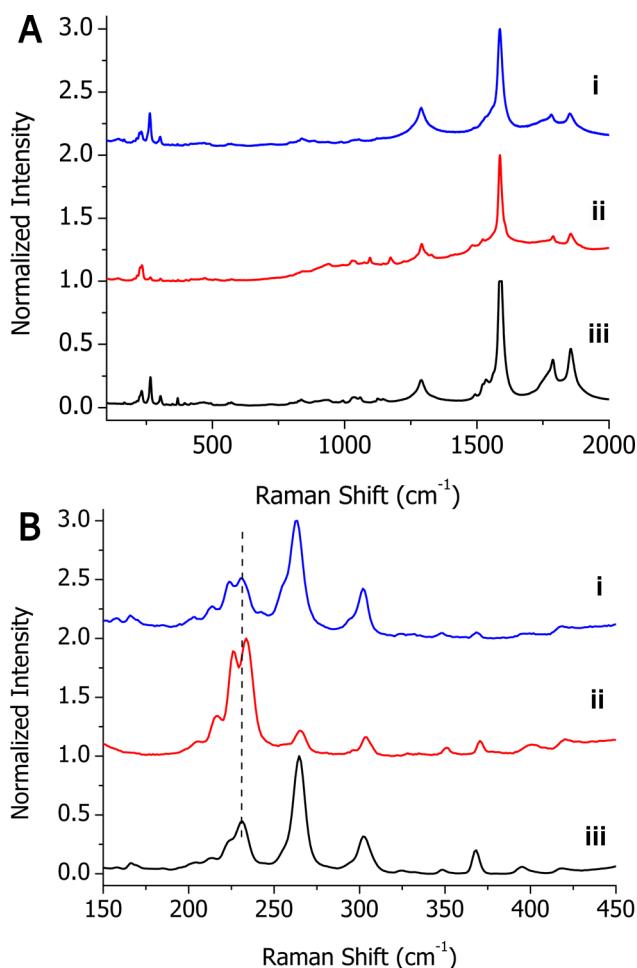
Figure 10. Raman spectra (A) of (i) raw CoMoCAT SWNTs, (ii) a copolymer **7**−CoMoCAT SWNT complex, and (iii) released CoMoCAT SWNTs. The expanded RBM region from the same data is given in (B). Samples were prepared by drop-casting dispersions onto silicon wafers followed by air-drying overnight and were excited at 785 nm.

reappearance of the bundling peak and a blue shift of the peak at 233 cm^{-1} back to 230 cm^{-1}, where it was in the original starting material. The shoulder peak at 225 cm^{-1} retained its relative intensity with respect to the 230 cm^{-1} signal, indicating that the enrichment of this nanotube species persisted in the nanotube sample recovered upon release. The signal at 301 cm^{-1} was found to mirror the one at 264 cm^{-1}, with a significant decrease in relative intensity upon interaction with copolymer **7** and then a recovery upon release of the nanotubes (Figure 10B). Similar data were observed with the **7**−HiPco complexes using 785 nm excitation (Figure S6, Supporting Information).

The thermal stability of copolymer **7**, the polymer−SWNT supramolecular complexes, and released SWNTs was characterized by thermogravimetric analysis (TGA), carried out under an Ar atmosphere. These data are shown in Figure 11 and indicate that the major mass loss for the copolymer occurs at 234 °C, amounting to 47%. This mass loss corresponds to the loss of side chains ($-SC_8H_{17}$) within the polymer. For the polymer−SWNT complex, the mass loss amounts to 30%, which indicates that the SWNT composition within the polymer−SWNT complexes was approximately 45%. The thermogram for the SWNTs that were released from the
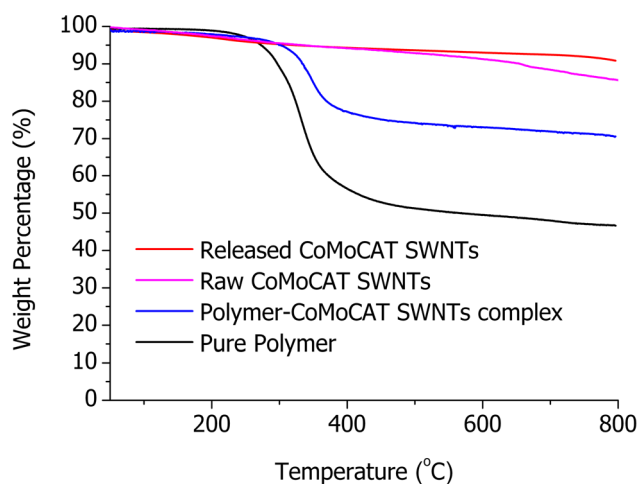
Figure 11. TGA profiles showing mass loss upon heating for copolymer **7**, **7**–SWNT complexes, raw SWNT, and released SWNT samples under Ar.

copolymer shows no appreciable mass loss up to 800 °C. This experiment definitively proves that the released SWNTs do not have any polymer on their surface and supports the hypothesis that the copolymer is able to completely desorb from the nanotube surface upon application of a stimulus, namely, TFA. Interestingly, comparison of the TGA data for the original, as-received CoMoCat sample with those for the released nanotubes after dispersion with copolymer **7** shows some difference. The original sample exhibits a reproducible mass loss with an onset temperature of around 600 °C. Considering that SWNTs should be stable to beyond 800 °C, this mass loss is attributed to impurities present in the as-received commercial sample. Several TGA measurements on this commercial batch of CoMoCAT SWNTs revealed identical data. Surprisingly, when TGA is carried out on the nanotubes released from copolymer **7**, as described above, the thermogram exhibits a lower mass loss upon heating to 800 °C. This indicates that dispersion with the copolymer is selective for SWNTs and results in exclusion of any amorphous carbon impurities and metal catalyst particles that were present in the original sample, thus leading to enrichment of the SWNT sample. It is evident that the purity of the nanotubes released from the copolymer is improved relative to that of this commercial sample.

Since SWNTs can rapidly and cleanly be released from the copolymer solution triggered by addition of TFA, the solubility of SWNTs in the polymer–SWNT dispersion in toluene can be easily determined. Upon addition of TFA, the resulting mixture was subjected to ultracentrifugation, and the SWNTs underwent membrane filtration and extensive washing with toluene. The released SWNTs were slowly stirred in aqueous $NaHCO_3$ solution to neutralize any protonation of SWNTs that may have happened during the release experiment.[56] The resulting isolated neutralized SWNTs were dried to constant mass. The recovered amounts of CoMoCat and HiPco SWNTs were 1.1 and 2.0 mg, respectively. This indicates that the concentrations in the original solutions (10 mL volume) were approximately 0.1 and 0.2 mg/mL for CoMoCat and HiPco SWNTs, respectively, when the concentration of copolymer was 5 mg/mL.

■ CONCLUSIONS

The synthesis of a novel conformationally switchable conjugated copolymer consisting of alternating TTFV and fluorene units was achieved. Absorption spectroscopy indicated that the polymer undergoes a two-step protonation process with TFA, accompanied by dramatic conformational changes in the polymer structure. This polymer exhibits strong interactions with the surface of SWNTs, allowing their homogeneous dispersion in a variety of organic solvents, including toluene, THF, and chloroform. Furthermore, the interaction of the copolymer with SWNTs was found to be size-selective, with a preference for low-diameter semiconducting SWNTs. Upon addition of TFA to the copolymer–SWNT dispersion, a rapid color change and simultaneous precipitation of the nanotube material were observed. From TGA measurements, it was found that the precipitated nanotubes were free of polymer, indicating that the polymer underwent the expected conformational change and desorbed from the nanotube surface upon protonation. Furthermore, on the basis of TGA data, the nanotube material isolated after the dispersion/release procedure was of higher purity than the SWNT starting material. It should also be noted that the polymer could be easily recovered and reused. This work demonstrates the feasibility of selectively dispersing a specific subpopulation of SWNTs from an impure mixture and their rapid, facile release and isolation in pure form upon application of a simple release trigger (acidification). Our work has significant implications for future nanotube enrichment/purification procedures, in terms of both nanotube chirality and overall separation from non-nanotube impurities.

■ ASSOCIATED CONTENT

⑤ Supporting Information
Full experimental details, PLE map for HiPco SWNTs dispersed with SDBS, AFM data, nanotube dispersion images, NMR data for the recovered polymer, and Raman data for the copolymer and copolymer-dispersed HiPco SWNTs. This material is available free of charge via the Internet at http://pubs.acs.org.

■ AUTHOR INFORMATION

Corresponding Author
adronov@mcmaster.ca
Notes
The authors declare no competing financial interest.

■ ACKNOWLEDGMENTS

■ REFERENCES

(1) Hirsch, A. *Angew. Chem., Int. Ed.* **2002**, *41*, 1853−1859.
(2) Hirsch, A.; Vostrowsky, O. *Top. Curr. Chem.* **2005**, *245*, 193−237.
(3) Bahr, J. L.; Tour, J. M. *J. Mater. Chem.* **2002**, *12*, 1952−1958.
(4) Rana, S.; Cho, J. W. *Nanoscale* **2010**, *2*, 2550−2556.
(5) Hu, C.-Y.; Xu, Y.-J.; Duo, S.-W.; Zhang, R.-F.; Li, M.-S. *J. Chin. Chem. Soc.* **2009**, *56*, 234−239.

(6) Grossiord, N.; Loos, J.; Regev, O.; Koning, C. E. *Chem. Mater.* **2006**, *18*, 1089−1099.

(7) Dyke, C.; Tour, J. *J. Phys. Chem. A* **2004**, *108*, 11151−11159.

(8) Tasis, D.; Tagmatarchis, N.; Bianco, A.; Prato, M. *Chem. Rev.* **2006**, *106*, 1105−1136.

(9) Schnorr, J. M.; Swager, T. M. *Chem. Mater.* **2011**, *23*, 646−657.

(10) Singh, P.; Campidelli, S.; Giordani, S.; Bonifazi, D.; Bianco, A.; Prato, M. *Chem. Soc. Rev.* **2009**, *38*, 2214−2230.

(11) Britz, D.; Khlobystov, A. *Chem. Soc. Rev.* **2006**, *35*, 637−659.

(12) Liu, P. *Eur. Polym. J.* **2005**, *41*, 2693−2703.

(13) Zhao, Y.-L.; Stoddart, J. F. *Acc. Chem. Res.* **2009**, *42*, 1161−1171.

(14) Guo, Z.; Feng, Y.; Zhu, D.; He, S.; Liu, H.; Shi, X.; Sun, J.; Qu, M. *Adv. Funct. Mater.* **2013**, *23*, 5010−5018.

(15) Park, S.; Lee, H. W.; Wang, H.; Selvarasah, S.; Dokmeci, M. R.; Park, Y. J.; Cha, S. N.; Kim, J. M.; Bao, Z. *ACS Nano* **2012**, *6*, 2487−2496.

(16) Pang, X.; Imin, P.; Zhitomirsky, I.; Adronov, A. *J. Mater. Chem.* **2012**, *22*, 9147−9154.

(17) Pang, X.; Imin, P.; Zhitomirsky, I.; Adronov, A. *Macromolecules* **2010**, *43*, 10376−10381.

(18) Dalton, A. B.; Stephan, C.; Coleman, J. N.; McCarthy, B.; Ajayan, P. M.; Lefrant, S.; Bernier, P.; Blau, W. J.; Byrne, H. J. *J. Phys. Chem. B* **2000**, *104*, 10012−10016.

(19) Star, A.; Stoddart, J. F.; Steuerman, D.; Diehl, M.; Boukai, A.; Wong, E. W.; Yang, X.; Chung, S.-W.; Choi, H.; Heath, J. R. *Angew. Chem., Int. Ed.* **2001**, *113*, 1771−1775.

(20) Star, A.; Stoddart, J. *Macromolecules* **2002**, *35*, 7516−7520.

(21) Star, A.; Liu, Y.; Grant, K.; Ridvan, L.; Stoddart, J. F.; Steuerman, D. W.; Diehl, M. R.; Boukai, A.; Heath, J. R. *Macromolecules* **2003**, *36*, 553−560.

(22) Cheng, F.; Adronov, A. *Chem.—Eur. J.* **2006**, *12*, 5053−5059.

(23) Cheng, F.; Imin, P.; Maunders, C.; Botton, G.; Adronov, A. *Macromolecules* **2008**, *41*, 2304−2308.

(24) Imin, P.; Imit, M.; Adronov, A. *Macromolecules* **2012**, *45*, 5045−5050.

(25) Chen, F.; Wang, B.; Chen, Y.; Li, L. *Nano Lett.* **2007**, *7*, 3013−3017.

(26) Nish, A.; Hwang, J.; Doig, J.; Nicholas, R. *Nat. Nanotechnol.* **2007**, *2*, 640−646.

(27) Hwang, J.-Y.; Nish, A.; Doig, J.; Douven, S.; Chen, C.-W.; Chen, L.-C.; Nicholas, R. *J. Am. Chem. Soc.* **2008**, *130*, 3543−3553.

(28) Stürzl, N.; Hennrich, F.; Lebedkin, S.; Kappes, M. M. *J. Phys. Chem. C* **2009**, *113*, 14628−14632.

(29) Gao, J.; Kwak, M.; Wildeman, J.; Herrmann, A.; Loi, M. *Carbon* **2010**, *49*, 333−338.

(30) Ozawa, H.; Ide, N.; Fujigaya, T.; Niidome, Y.; Nakashima, N. *Chem. Lett.* **2011**, *40*, 239−241.

(31) Lemasson, F. A.; Strunk, T.; Gerstel, P.; Hennrich, F.; Lebedkin, S.; Barner-Kowollik, C.; Wenzel, W.; Kappes, M. M.; Mayor, M. *J. Am. Chem. Soc.* **2011**, *133*, 652−655.

(32) Lemasson, F.; Berton, N.; Tittmann, J.; Hennrich, F.; Kappes, M. M.; Mayor, M. *Macromolecules* **2012**, *45*, 713−722.

(33) Lee, H. W.; Yoon, Y.; Park, S.; Oh, J. H.; Hong, S.; Liyanage, L. S.; Wang, H.; Morishita, S.; Patil, N.; Park, Y. J.; Park, J. J.; Spakowitz, A.; Galli, G.; Gygi, F.; Wong, P. H. S.; Tok, J. B.-H.; Kim, J. M.; Bao, Z. *Nat. Commun.* **2011**, *2*, 541−548.

(34) Imin, P.; Imit, M.; Adronov, A. *Macromolecules* **2011**, *44*, 9138−9145.

(35) Wang, W. Z.; Li, W. F.; Pan, X. Y.; Li, C. M.; Li, L.-J.; Mu, Y. G.; Rogers, J. A.; Chan-Park, M. B. *Adv. Funct. Mater.* **2011**, *21*, 1643−1651.

(36) Lemasson, F.; Tittmann, J.; Hennrich, F.; Stürzl, N.; Malik, S.; Kappes, M. M.; Mayor, M. *Chem. Commun.* **2011**, *47*, 7428.

(37) Liang, S.; Chen, G.; Peddle, J.; Zhao, Y. *Chem. Commun.* **2012**, *48*, 3100−3102.

(38) Liang, S.; Chen, G.; Zhao, Y. *J. Mater. Chem. C* **2013**, *1*, 5477−5490.

(39) Chen, G.; Mahmud, I.; Dawe, L. N.; Zhao, Y. *Org. Lett.* **2010**, *12*, 704−707.

(40) Yamashita, Y.; Tomura, M.; Badruz Zaman, M. *Chem. Commun.* **1998**, 1657−1658.

(41) Yamashita, Y.; Tomura, M.; Tanaka, S.; Imaeda, K. *Synth. Met.* **1999**, *102*, 1730−1731.

(42) Hascoat, P.; Lorcy, D.; Robert, A.; Carlier, R.; Tallec, A.; Boubekeur, K.; Batail, P. *J. Org. Chem.* **1997**, *62*, 6086−6089.

(43) Guerro, M.; Carlier, R.; Boubekeur, K.; Lorcy, D.; Hapiot, P. *J. Am. Chem. Soc.* **2003**, *125*, 3159−3167.

(44) Bouzan, S.; Chen, G.; Mulla, K.; Dawe, L. N.; Zhao, Y. *Org. Biomol. Chem.* **2012**, *10*, 7673−7676.

(45) Kirketerp, M.-B. S. M.; Leal, L. A. E. L.; Varsano, D. D.; Rubio, A. A.; Jørgensen, T. J. D. T.; Kilså, K. K.; Nielsen, M. B. M.; Nielsen, S. B. S. *Chem. Commun.* **2011**, *47*, 6900−6902.

(46) Zhao, Y.; Chen, G.; Mulla, K.; Mahmud, I.; Liang, S.; Dongare, P.; Thompson, D. W.; Dawe, L. N.; Bouzan, S. *Pure Appl. Chem.* **2012**, *84*, 1005−1025.

(47) O'Connell, M.; Bachilo, S.; Huffman, C.; Moore, V.; Strano, M.; Haroz, E.; Rialon, K.; Boul, P.; Noon, W.; Kittrell, C.; Ma, J.; Hauge, R.; Weisman, R.; Smalley, R. *Science* **2002**, *297*, 593−596.

(48) Bachilo, S.; Strano, M.; Kittrell, C.; Hauge, R.; Smalley, R.; Weisman, R. *Science* **2002**, *298*, 2361−2366.

(49) Rao, A.; Richter, E.; Bandow, S.; Chase, B.; Eklund, P.; Williams, K.; Fang, S.; Subbaswamy, K.; Menon, M.; Thess, A.; Smalley, R.; Dresselhaus, G.; Dresselhaus, M. *Science* **1997**, *275*, 187−191.

(50) Dresselhaus, M. S.; Eklund, P. C. *Adv. Phys.* **2000**, *49*, 705−814.

(51) Dresselhaus, M. S.; Dresselhaus, G.; Jorio, A.; Souza Filho, A. G.; Pimenta, M. A.; Saito, R. *Acc. Chem. Res.* **2002**, *35*, 1070−1078.

(52) Fantini, C.; Jorio, A.; Souza, M.; Strano, M. S.; Dresselhaus, M. S.; Pimenta, M. A. *Phys. Rev. Lett.* **2004**, *93*, 1−4.

(53) O'Connell, M.; Sivaram, S.; Doorn, S. *Phys. Rev. B* **2004**, *69*, 235415.

(54) Luo, Z.; Doorn, S. K.; Li, R.; Papadimitrakopoulos, F. *Phys. Status Solidi B* **2006**, *243*, 3155−3160.

(55) Jiang, C.; Saha, A.; Xiang, C.; Young, C. C.; Tour, J. M.; Pasquali, M.; Martí, A. A. *ACS Nano* **2013**, *7*, 4503−4510.

(56) Engtrakul, C.; Davis, M. F.; Gennett, T.; Dillon, A. C.; Jones, K. M.; Heben, M. J. *J. Am. Chem. Soc.* **2005**, *127*, 17548−17555.